International Journal of Fluid Machinery and Systems
Vol. 2, No. 1, January-March 2009

Original Paper

Prediction of Specific Noise Based on Internal Flow of Forward Curved Fan

Soichi Sasaki[1], Hidechito Hayashi[1] and Makoto Hatakeyama[2]

[1]Department of Mechanical Systems Engineering, Nagasaki University
1-14 Bunkyo-machi, Nagasaki, 852-8521, Japan
[2]Products R&D Department, TOTO LTD. Research Institute
2-8-1 Honson, Chigasaki, 253-8577, Japan

Abstract

In this study, a prediction theory for specific noise that is the overall characteristic of the fan has been proposed. This theory is based on total pressure prediction and broadband noise prediction. The specific noises of two forward curved fans with different number of blades were predicted. The flow around the impeller having 120 blades (MF120) was more biased at a certain positions than the impeller with 40 blades (MF40). An effective domain of the energy conversion of MF40 has extended overall than MF120. The total pressure was affected by the slip factor and pressure loss caused by the vortex flow. The suppression of a major pressure drop by the vortex flow and expansion of the effective domain for energy conversion contributed to an increase in the total pressure of MF40 at the design point. The position of maximum relative velocity was different for each fan. The relative velocity of MF120 was less than that of MF40 due to the deviation angle. The specific noise of MF120 was 2.7 dB less than that of MF40 due to the difference in internal flow. It has been quantitatively estimated that the deceleration in the relative velocity contributed to the improvement in the overall performance.

Keywords: Centrifugal Fan, Internal Flow, Wake, Vortex, Pressure Drop, Aerodynamic Noise

1. Introduction

Forward curved fans are widely used in common household appliances such as air conditioners, kitchen ventilators, and bathroom dryers. Since these appliances are often driven continuously for a long periods, to be aerodynamically high efficiency is demanded from the viewpoint in the energy resource. In 2003, the Japanese government revised the Building Standard Law in order to take into account the "sick house syndrome". The revision in the law made it mandatory for ventilation equipment to be continuously operated for 24 h. Thus, it became necessary not only to increase fan efficiency but also to decrease fan noise in order to ensure a comfortable living environment. At the same operation point, the absolute velocity of the forward curved fan, which has an impeller with a forward curved blade, is theoretically greater than that of a turbofan, which has a backward curved impeller. This causes an increase in the pressure loss, although the total pressure increases at the design point. Therefore, the operating range of forward curved fans at high pressures is narrower than that of turbofans, and the efficiency of forward curved fans in this operation range is also low. Further, the level of the fan noise is observed to increase with the mean velocity when the total pressure on the fan is high.

Specific noise is a characteristic that is related to the aerodynamic characteristics of the fan and its noise level. The specific noise means the noise level per unit flow rate and per unit total pressure. The Japanese Standards Association [1] defines specific noise as shown in eq. (1).

$$L_{SA} = L_A + 10 \log (Q\, P_t^2) + 20 \tag{1}$$

where L_A is the A-weighted sound pressure level of the fan (dB), Q is the flow rate (m^3/min), and P_t is the total pres sure (Pa). In order to accurately predict the specific noise of the fan, first of all, it is necessary to quantitatively estimate the relation between the internal flow phenomena and the pressure loss. Kind et al. [2] studied the experimental characteristics of a separation domain produced by a vortex flow at the front side of the impeller. However, there have been few practical studies on the quantitative influence of flow phenomena such as vortex flow on pressure loss [3]. On the other hand, many studies about the experimental characteristics of the noise of a forward curved fan have been reported [4], [5], [6]. In the case of a multiblade

Received July 9 2009; revised February 4 2009; accepted for publication February 6 2009: Review conducted by Prof. Yang Bo-suk. (Paper number O08015)
Corresponding author: Sohichi Sasaki, Assistant Professor, souichi@nagasaki-u.ac.jp

impeller, the interference between the blade and wake vortex has a considerable influence on noise prediction since the pitch of the blade is narrow. Further, during actual operating conditions, aerodynamic noise occurring in the broadband frequency domain is found to be the predominant contributing factor to fan noise. However, practical examples of the prediction of broadband noise using the characteristics of the wake vortex have been few. These abovementioned situations hamper efforts for accurate prediction of the specific noise of the fan.

In this study, a prediction theory of the specific noise of a forward curved fan is proposed. This theory is composed of the prediction of total pressure and broadband noise. In order to predict the total pressure, a quantitative analysis method to determine the pressure loss caused by the vortex flow is proposed. Further, the prediction equation of the spectrum distribution of the broadband noise with the characteristics of the wake vortex is derived. Finally, the influence of internal flow on the specific noise of the forward curved fan is discussed based on the characteristics estimated by this theory.

2. Experimental Apparatus and Measurement Method

The test impeller is shown in Fig.1 and its main dimensions are summarized in Table 1. These impellers are the forward curved centrifugal type. The fan is designed taking into consideration the number of blades of the impeller; fans with 40 and 120 blades are referred to as MF40 and MF120, respectively.

(a) MF40 (b) MF120

Fig. 1 Impeller

Table 1 Main dimensions of the test impeller

Impeller	MF40	MF120
Number of blades , B	40	120
Inner diameter , D_1 (mm)	110	
Outer diameter , D_2 (mm)	125	
Chord length , C (mm)	8	
Inlet angle , β_{b1} (deg.)	64.7	
Outlet angle , β_{b2} (deg.)	152.6	
Span length , b_2 (mm)	50	
Thickness , t (mm)	1	

The experimental apparatus used for measuring the aerodynamic characteristics of the fan is shown in Fig. 2. The main dimensions of the scroll casing are summarized in Table 2. A duct with a length of 1248 mm is attached to the exhaust port of the fan. The static pressure is measured by a pressure tap placed 80 mm below the fan exit on the downstream side. This measurement method of the pressure characteristics of the fan is different from the industrial standard, for instance JIS. However, when the pressure characteristics is measured based on the above mentioned method, the pressure characteristic of the fan is given the various pressure drops by the duct, the honeycomb, the orifice and so on. Therefore, in this study, the pressure characteristic obtained at the vicinity of the fan exit is discussed. The total pressure is defined as the sum of the dynamic pressures estimated by considering the mean velocity in the duct and the measured static pressure. The flow rate is measured by an orifice plate placed at a distance of 873 mm from the exit. The flow rate is controlled by a damper set up near the exit of a subsidiary fan. The flow coefficient ϕ and the total pressure coefficient ψ_t are defined as in eq. (2).

$$\phi = \frac{Q}{60\pi D_2 b_2 u_2}, \psi_t = \frac{2P_t}{\rho u_2^2} \tag{2}$$

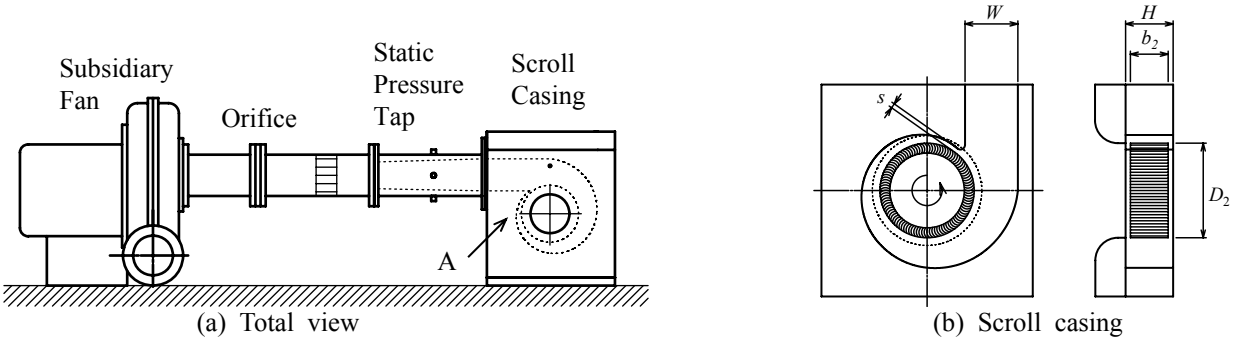

(a) Total view (b) Scroll casing

Fig. 2 Experimental apparatus for measuring aerodynamic characteristics

Table 2 Main dimensions of the scroll casing

Volute angle, θ_v (deg.)	6.0
Clearance, s (mm)	6.0
Duct size, W (mm) × H (mm)	70 × 63

where Q is the flow rate (m^3/min) and P_t is the total pressure (Pa). The distance between the point of measurement of the internal flow and the center of the motor axis was 72.5 mm. A five-hole Pitot tube was used to measure the absolute flow velocity, the static pressure, and the absolute flow angle at the impeller outlet. In order to determine the measurement point to the blade span direction, the nine points which divided equivalently with 5 mm pitch from the front side to the rear side is employed.

Figure 3 shows the experimental apparatus for measuring the fan noise. The fan noise was measured in an anechoic room; the background noise in the room was below 25 dB in the A-weight measurement. In order to intercept the electric noise and mechanical noise from the motor, the motor is stored in an aluminum box; the interior of the box is covered with a rubber soundproof material. The flow rate of the fan was adjusted according to the static pressure specified by the *P-Q* characteristics. The noise was measured at an observation point that was 1.0 m above the bell mouth situated along the axis of the motor. The whole experiment was performed at a speed of 2800 rpm.

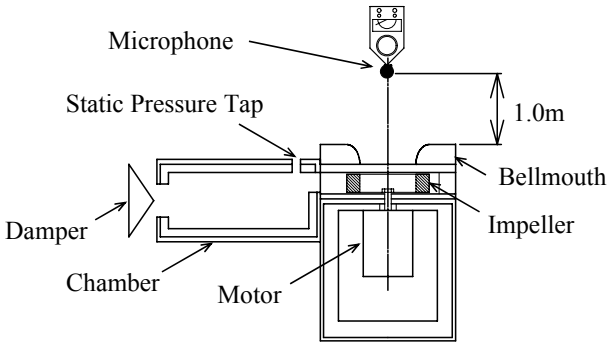

Fig. 3 Experimental apparatus for the measuring the aerodynamic noise

3. Prediction Theory of Specific Noise

3.1 Prediction of Total Pressure

The biased flow model around the impeller is shown in Fig. 4. The existence of a biased flow in the forward curved fan in the vicinity of the measurement position MP, which is shown in the figure, has been proved experimentally in reference [7]. It should be noted that it is not possible to measure the complete circumferential distribution of the flow around the impeller since the width of the channel in the scroll casing is narrow in the vicinity of the volute tongue. Therefore, in the experimental study, it becomes necessary to presume a suitable scale for the estimate of the biased flow. The measured flow rate in one pitch and the designed flow rate are indicated in eq. (3).

$$dq = \frac{\pi D_2}{B}\int_z v_{r2}(z)\,dz \;,\; dQ = \frac{\pi\ D_2\ b_2\ u_2\ \phi}{B} \tag{3}$$

where dq is the measured flow rate in a blade pitch and dQ is the designed flow rate. The measured and design values of the total flow rate of the impeller should be equal although the value of the actual measured flow rate dq is found to be greater than the designed value dQ because of the biased flow, i.e., it is considered that the flow rate at other positions is underestimated because of the large flow rate in the vicinity of MP. K_θ in eq. (4) is a coefficient used to indicate the ratio of the scales of such a biased flow.

$$K_\theta = 1 - \frac{dQ}{dq} \tag{4}$$

where K_θ is defined as the biased flow coefficient.

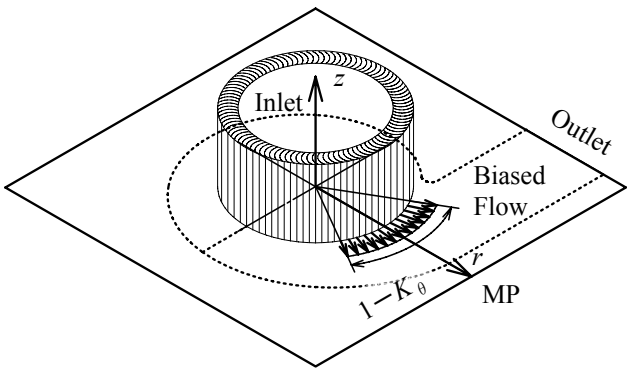

Fig. 4 Model of the biased flow around the impeller

A model of the vortex flow in the scroll casing in the vicinity of MP is shown in Fig. 5. Figure 5(a) shows the total view, and Fig. 5(b) shows the meridional section (*r-z* section). The flow in the model has been divided into two domains—a vortex flow domain where the vortex flow is biased toward the front side, and a main flow domain where the outflow is biased toward the

rear side. The ratio of the scale of the vortex flow domain to the blade span, i.e., the blockage factor K_z, is estimated by eq.(5), which is based on the concept of the displacement thickness of the radial flow velocity.

$$K_z = \frac{1}{b_2}\int_0^{b_2}\left(1-\frac{v_{r2}(z)}{\overline{v_{r2}}}\right)dz \tag{5}$$

where $v_{r2}(z)$ is the radial flow velocity distribution at the impeller outlet and $\overline{\ }$ denotes the ensemble average in the main flow domain. The blockage factor K_z is defined as the vortex flow coefficient.

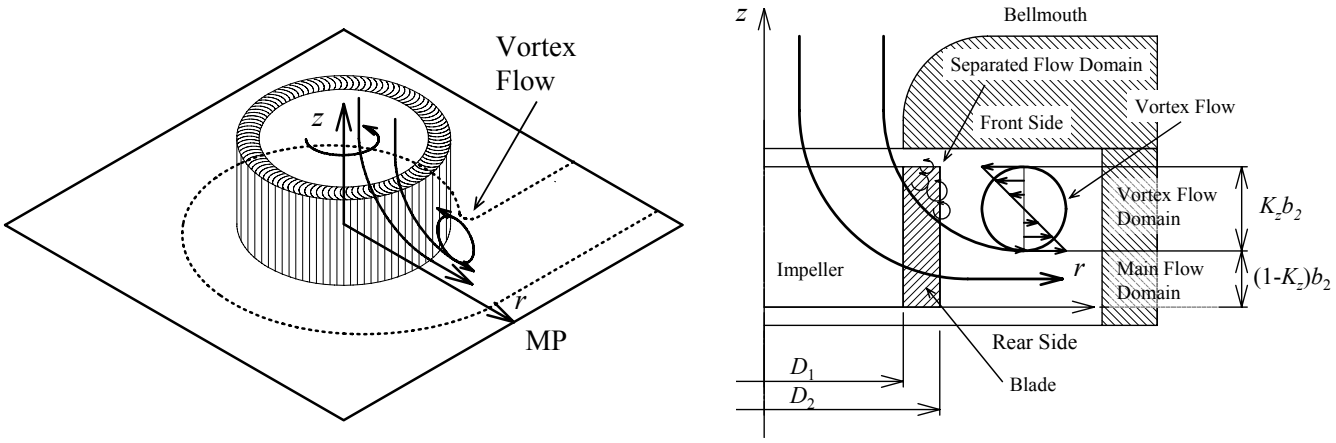

(a) Total view (b) Meridional section

Fig. 5 Schematic view of the vortex flow in the meridional section

The velocity triangles at the inlet and outlet of the impeller in the main flow domain are given in Fig. 6. The flow at the inlet has no prewhirls. The flow between the blades forms a boundary layer on the pressure surface side (*PS* side). On the suction surface side (*SS* side), the flow reattached at the leading edge also forms a boundary layer and is separated again at a separation point. Then, the slip factor at the exit of the impeller is given by eq. (6).

$$k_2 = c_{sl2}/u_2 \quad , c_{sl2} = \sqrt{{w_{2\infty}}^2 + {w_2}^2 - 2w_{2\infty}w_2\cos\gamma_2} \tag{6}$$

The designed shape of the arc blade is shown in Fig. 7. The separation point at the *SS* side has been determined to be the point where the stream lines B, which has a deviation angle γ_2, and the arc A come in contact with each other. The length of the separation domain L is determined by eq. (7).

$$L = \left| \overrightarrow{l_2} - \overrightarrow{l_S} \right| \tag{7}$$

where l_2 is the vector defined from the center of the arc to the trailing edge and l_S is the vector defined from the center to the separation point.

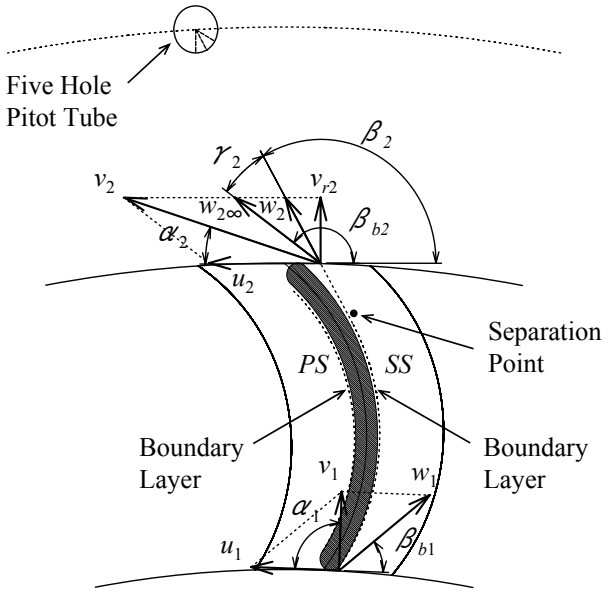

Fig. 6 Velocity triangles

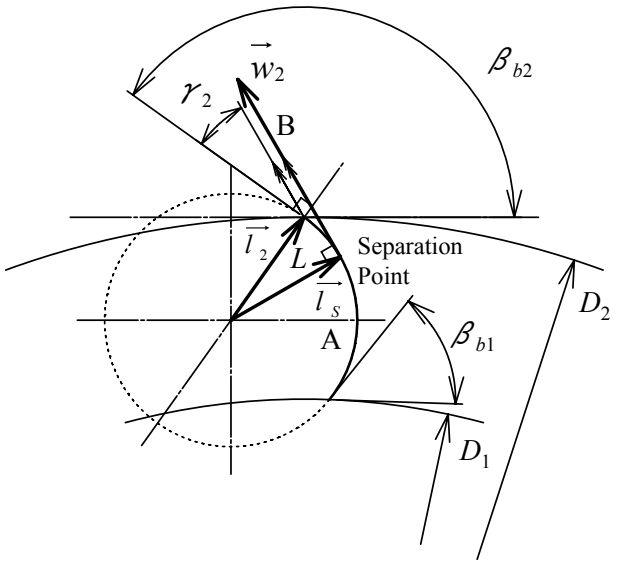

Fig. 7 Designed shape of the arc blade

The vector of the relative flow velocity at the impeller outlet is shown in Fig. 8. The boundary layer displacement thickness of both sides (*PS* and *SS*) and the width of the shear layer on the *SS* side are expressed in eq. (8).

$$\delta_{PS} = 0.0477\ C\ Re^{-1/5}\ , \delta_{SS} = 0.0477\ \xi\ Re_{\xi}^{\ -1/5}\ ,\ D_{SS} = L \sin\gamma_2 \tag{8}$$

where

$$Re = w_2\ C / \nu\ , Re_{\xi} = w_2\ \xi / \nu\ ,\ \xi = C - L$$

In the above equations, δ is the displacement thickness of the turbulent boundary layer and its value is determined using the 1/7 power law [8]. D_{SS} is the width of the shear layer on the *SS* side, w_2 is the relative flow velocity at the impeller outlet, and $R_{e\xi}$ is the Reynolds number based on the domain of the boundary layer on the *SS* side. From the aforementioned assumption, we derive the width of the wake D^* as shown in eq.(9).

$$D^*_2 = 0.8\ (\delta_{PS} + t + D_{SS} + \delta_{SS}) \tag{9}$$

where *t* is the thickness of blade.

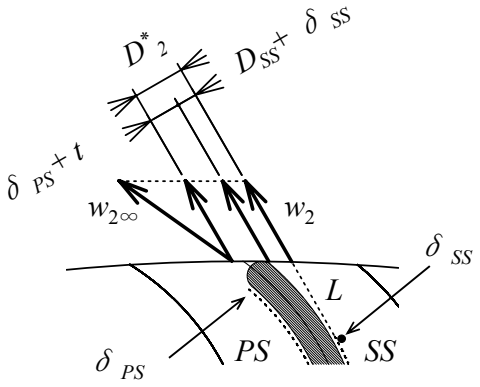

Fig. 8 Velocity vector of the relative velocity and the width of the wake

The pressure loss head proposed by Johnston and Dean [9] is calculated by estimating the head caused by mixing and diffusion of the wake.

$$\Delta h_w = \left(\frac{K_w}{1-K_w}\right)^2 \frac{v_{r2}^{*\,2}}{2g} \tag{10}$$

where,

$$v_{r2}^{\ *} = (1-K_\theta)v_{r2}\ ,\ K_w = \frac{D^*_2}{S}$$

Here, K_w is the ratio of the width of the wake to the blade pitch (wake coefficient) and *S* is the pitch of the blade. In the next section, all the variables indicated with an asterisk (*) indicate parameters that have uniform flow properties with the exception of the variable D^*.

Figure 9 is the flow model for the section from MP to the exit of the fan. Figure 9(a) shows the flow in the exhaust duct in the horizontal plane, and Fig. 9(b) shows the flow in the vertical plane. When the direction of the flow in the vortex flow domain is changed compulsory toward the duct by the volute tongue, the flow in the main flow domain mixes (and diffuses) with the flow in the vortex flow domain. The areas of the entrance section and the exhaust section in the control volume of the duct are given by

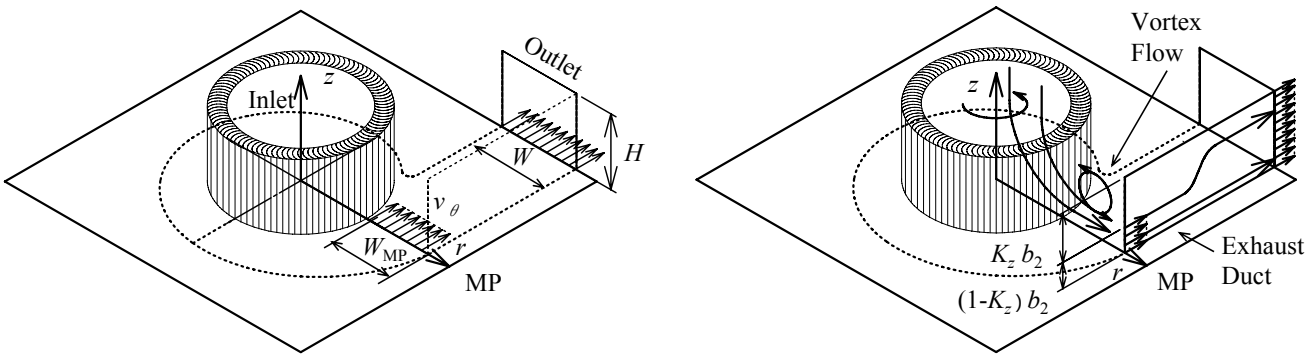

(a) Horizontal view (b) Vertical view

Fig. 9 Flow pattern in the exhaust duct of the scroll casing

eq. (11) as follows:

$$A_1 = K_r\ (1-K_z)HW\ ,\ A_2 = H\ W\ ,\ K_r = \frac{W_{MP}}{W} \tag{11}$$

where A_1 is the area of MP, K_r is the projection ratio of the impeller, H is the height of the scroll casing, W is the width of the casing at the exit of the fan, A_2 is the area of the exit of the fan, and W_{MP} is the width of the casing at MP. When the pressure loss of the sudden expansion is assumed to the control volume, the pressure loss head caused by the vortex flow in the volume can be given by eq. (12).

$$\Delta h_{vf} = \left(1 - K_r + K_r\ K_z\right)^2 \frac{v_{\theta 2}^{*\ 2}}{2g} \tag{12}$$

where $v_{\theta 2}$ is the circumferential component of the absolute flow velocity. If the drop in pressure is normalized by the dynamic pressure head of the tangential velocity u_2, the total pressure coefficient can be expressed as given in eq. (13).

$$\phi_t = \phi_{th\infty} - 2k_2 - \sum \Delta\, \phi = \phi_{th} - \Delta\, \phi_{vf} - \Delta\, \phi_w \tag{13}$$

where

$$\phi_{th\infty} = 2\left(1 - \frac{v_{r2}^{*}}{u_2}\cot\beta_{b2}\right)$$

In the above equations, $\psi_{th\infty}$ is Euler's total pressure coefficient, k_2 is the slip factor, $\Sigma \triangle\psi$ is the total pressure loss coefficient, and $\triangle\psi$ is the pressure loss coefficient.

3.2 Prediction of Fan Noise

The pressure fluctuation on the blade induced by a Karman vortex street is shown in Fig. 10. Figure 10(a) shows the pressure distribution in the direction of the main flow of the Karman vortex street, while Fig. 10(b) shows the pressure fluctuations at a certain position in the vicinity of the trailing edge. In this study, the ratio of vortex scale is defined in eq. (14) as the ratio of the diameter of the vortex to the width of the wake.

$$\varepsilon = d / D \tag{14}$$

where d is the diameter of the vortex and D is the width of the wake. The pressure fluctuations are influenced by the pressure distribution of the Rankin vortex. Theoretically, the ratio D/L in Fig. 10 becomes $D/L = 0.2806$ when the Karman vortex street is formed in the wake. Therefore, the intermittency ratio κ of the periodic phenomenon of vortex shedding in a cycle is given by eq. (15).

$$\kappa = \frac{d}{L} = \frac{D}{L}\frac{d}{D} = 0.2806\varepsilon \tag{15}$$

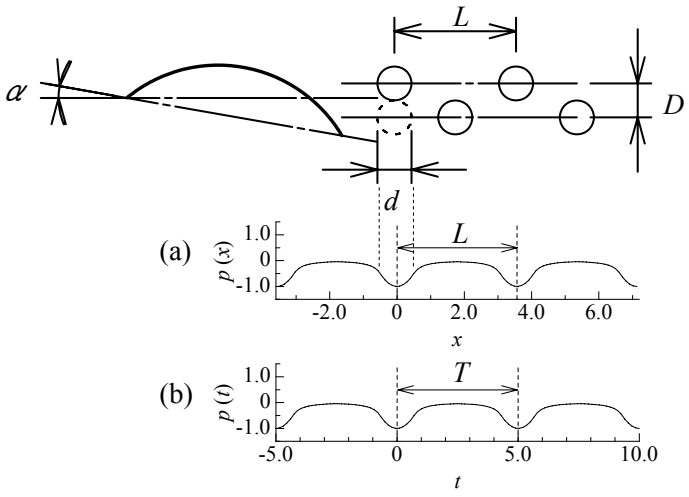

Fig. 10 Relation between the vortices in the Karman vortex street and the pressure characteristics

Fig. 11 shows the Karman vortex street in the near wake of the blade of the impeller. When the vortex is approximated to a Rankin vortex with diameter d, the pressure in the center of the vortex becomes negative (see Fig. 10). Thus, when the vortex is shed, a normal force is induced. In this study, the force induced by the vortex shedding is named as local lift. If the wake diffuses with a constant Strouhal number in the near field, the width of the wake can be divided into n pieces in the mainstream direction.

$$D^*_{\ j} = \frac{S_t\ w_2}{f_j}\ ,\ j = 2 \sim n \tag{16}$$

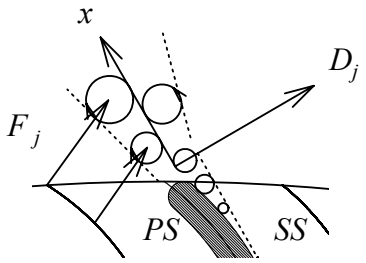

Fig. 11 Karman vortex street in the wake of the blade of the impeller

where f denotes the frequency of vortex shedding, S_t is the Strouhal number (S_t = 0.2), j is the counter for the discretization, and w_2 is the relative velocity of the rotational impeller. The circulation of the vortex when the diameter of the vortex rotates due to its own velocity fluctuations is given by eq. (17).

$$\overline{\Gamma} = \pi \, d \, \overline{w'} \tag{17}$$

where, $\overline{\ }$ denotes the symbol for root mean square, Γ is the circulation of the vortex, and w' is the velocity fluctuation. When the vortex with a circulation and an intermittency ratio κ is shed in the wake, a local lift is induced by the vortex. The lift on the blade surface is estimated by the Magnus effect, which is given by eq. (18).

$$\overline{F} = \kappa \, \rho \, \overline{w'} \, \overline{\Gamma} \, L_S \tag{18}$$

where L_S denotes the vortex scale in the span direction. Then, the lift coefficient normalized by the scale of this vortex is given as follows:

$$\overline{C_L} = \frac{\kappa \, \rho \, w_2 \, \overline{\Gamma} \, L_S}{\frac{\rho \, w^2}{2} \, d \, L_S} = \frac{2 \, \kappa \, \pi \, \overline{w'}}{w_2} \tag{19}$$

If a Karman vortex street exists in the near field of the impeller, a local lift is induced on the solid surface of the adjoining blades (see Fig. 11). An original equation of sound pressure has been presented by Curle [10]. Broadband noise is generated by the overlapping of sound pressures by these vortices. Equation (20) is a discretized equation of the sound pressure.

$$\overline{p} = \frac{1}{4 \, \pi \, a_0} \frac{r_i}{r^2} \frac{\overline{\partial F_{i\,j}}}{\partial t}, \tag{20}$$

where p is the sound pressure, a_0 is the speed of sound, r is the distance between the sound source and the observation point, i denotes a vector, and F is the local lift induced by a vortex. When the lift fluctuates with the sine wave, the lift coefficient is differentiated, and eq. (21) is obtained as follows:

$$\frac{\partial \, \overline{C_L}}{\partial t} = \omega \, \overline{C_L} \tag{21}$$

The angular velocity can be derived by eq. (22) related to the Strouhal number.

$$\omega = \frac{2 \, \pi \, S_t \, w_2}{D^*} \tag{22}$$

It has been experimentally proven that the vortex scale in the span direction is approximately three times the width of wake [11], [12], [13]. Thus, in this study, the aspect ratio of the vortex λ is theoretically given by eq. (23) by considering L_S as the wavelength of the Karman vortex street.

$$L_S = \lambda \, D = 3.564 \, D \, , \because \frac{D}{L_S} = 0.2806 \tag{23}$$

Then, the root mean square of the sound pressure is as follows:

$$\overline{p_j} = \frac{\varepsilon \, \rho \, {w_2}^3 \, S_t \, \lambda \, {D^*}_j \, \overline{C_L}}{4 \, a_0 \, r} \, , \, j = 2 \sim n \tag{24}$$

The spectral density of the fan noise is given as

$$L_{A\,j} = 10 \log \left(\frac{\overline{p_j}^2}{{p_o}^2} \right) - \Delta L_{A\,j} \tag{25}$$

where p_0 is the base sound pressure ($20 \, \mu$ Pa) and $\triangle L_{A\,j}$ is the A-weighted sound pressure level at the each frequency. Then, the overall sound pressure level that represents the fan noise is given by

$$L_A = 10\log\left(\sum_{j=2}^{n} 10^{\frac{L_{Aj}}{10}}\right) \tag{26}$$

3.2 Prediction of Specific Noise

The Japanese Standards Association [14] defines specific noise as

$$L_{SA} = L_A - 10\log(QP_t^2) + 20 \tag{27}$$

where Q is the flow rate (m^3/min) and P_t is the total pressure (Pa). By giving the flow rate coefficient of the design point to the eq. (13), the total pressure is obtained. The specific noise can be calculated from eq. (27) and takes into account the values of the designed flow rate, the total pressure calculated through eq. (13), and the fan noise calculated by eq. (26).

4. Results and Discussion

The distribution of the radial component of absolute velocity is shown in Fig. 12. Figure 12(a) shows the circumferential distribution of the velocity at z/b_2 = 0.4. The variable θ on the horizontal axis in this figure is the angle measured in the counterclockwise direction from the base of the angle at the point A, which is shown in Fig. 2. The point to measure the velocity is determined with reference to this velocity distribution. The biased flow coefficient K_θ implies that if the number is large, the flow of the fan is biased in a certain location. The velocity distribution of MF120 is more biased than that of MF40. Figure 12(b) compares the velocity distributions in the blade span. On the basis of the value of the vortex flow coefficient, it is observed that the radial velocity of MF40 is more biased toward the hub than that of MF120. An effective domain of the energy conversion of MF40 has extended overall than MF120.

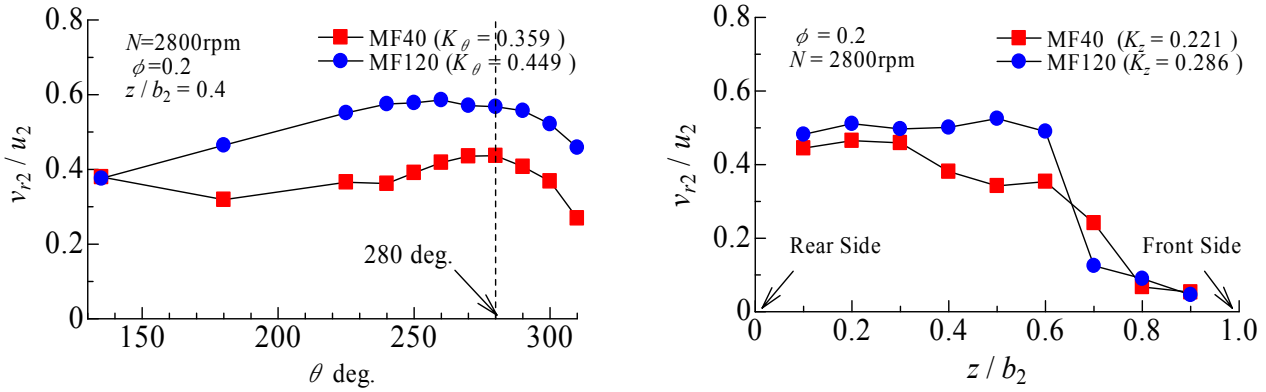

(a) Circumference direction (b) Span direction

Fig. 12 Distribution of the radial flow velocity

Figure 13 shows the measured characteristics and the predicted characteristics of the total pressure. In this analysis, the design point was set at ϕ = 0.2. The symbol of circle and square in the figure are the measured total pressure, the solid lines show the predicted characteristics and the thick broken line shows the characteristics of the total pressure in the atmospheric pressure at the outlet of the fan. In the domain from 0.15 until the design point, the total pressure characteristics estimated by eq. (13) can

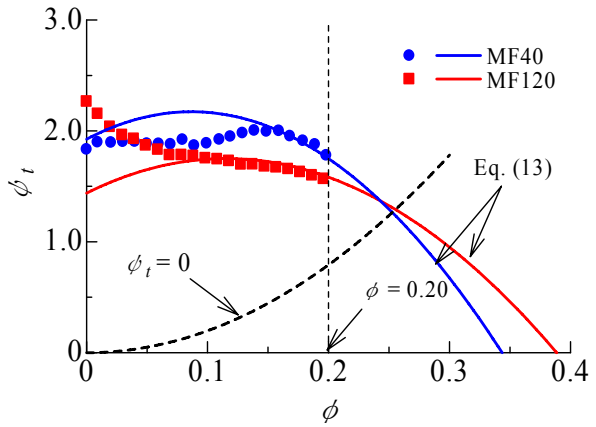

Fig. 13 Characteristics of the total pressure coefficient

Table 3 Summary of total pressure and the pressure drop

	MF40	MF120
ϕ	0.2	
ψ_{th}	2.12	2.20
$2k_2$	0.051	0.401
$\Delta\psi_w$	<0.01	0.018
$\Delta\psi_{vf}$	0.322	0.198
ψ_t (Prediction)	1.75	1.58
ψ_t (Measurement)	1.76	1.55

predict the tendencies of the actual measurements. However, in the domain where the flow coefficient was low, the predicted value of the total pressure coefficient did not correspond to its measured value. Thus, it is considered that the internal flow of the fan in the domain that has a low flow coefficient does not obey the flow model proposed in this study. Table 3 is a summary of the total pressure and the pressure drops. It has quantitatively clarified that the drop in pressure due to the vortex flow has a considerable influence on the pressure drop of the entire system.

The distribution of the relative velocity is shown in Fig.14. Figure 14 (a) shows the velocity distribution in the circumferential direction. It can be observed that the distribution of the internal flow is not uniform around the impeller and the value of the circumferential angle for which the velocity is maximum varies. The velocity distribution along the blade span is measured at the point where the maximum value of velocity can be obtained. Figure 14(b) shows the velocity distribution in the span direction. The maximum relative velocity of MF120 is found to be lower than that of MF40.

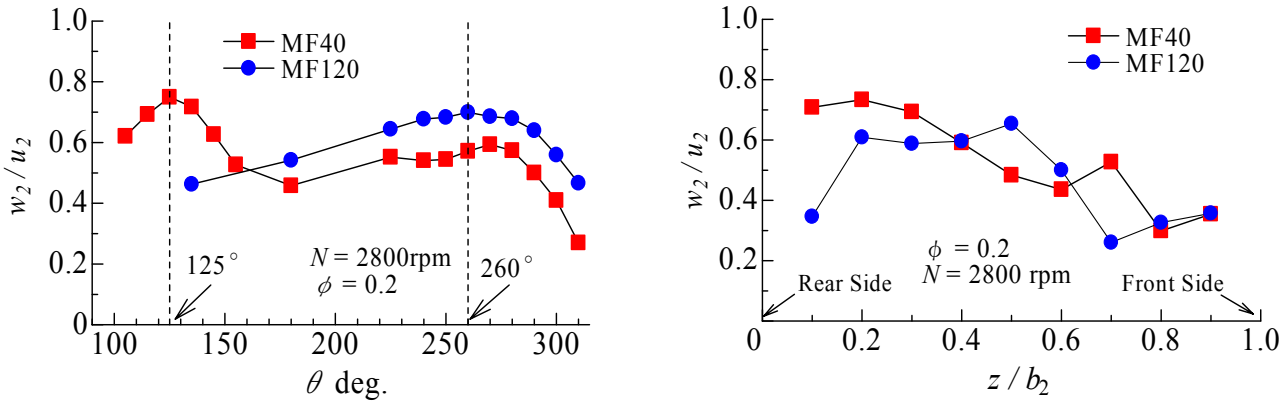

(a) Circumferential direction (b) Span direction

Fig. 14 Distribution of the relative velocity in the fan

The distributions of the deviation angles are compared in Fig. 15. The angle of MF40 is smaller than that of MF120 in the mainstream domain. As shown in Fig. 16, when the deviation angle of MF120 is larger than that of MF40 the slip velocity increases due to the presence of the forward curved blade. Therefore, the relative velocity of MF120 is less than that of MF40.

The spectrum distributions of the noise from each fan are compared in Fig. 17. The symbols of circle and square denote the measured spectra and the broken lines denote the predicted level. The parameters used for noise prediction are summarized in Table 4. The wake characteristics obtained from the wind tunnel test in reference [15] are used for noise prediction. Since the measured noise level is lower than the predicted level in the low frequency domain, it can be assumed that a Karman vortex street with this frequency is no longer formed in the wake. Therefore, the following noise levels are summarized by the overall level in the domain of $f >$ 1000 Hz. The spectrum distribution of the predicted values (broken line) can successfully estimate the broadband noise distributed in the 1000-3000Hz. The noise spectrum distribution is found to be fairly large in this domain. Therefore, in this case, the fan noise is found to be dominated by the broadband noise. The noise level of MF120 for the domains with a frequency above 1000 Hz is found to be smaller than that of MF40. Since the relative velocity was decelerated by the devi ation angle, it is considered that the noise level of MF120 is lower than that of MF40 (see Table 4).

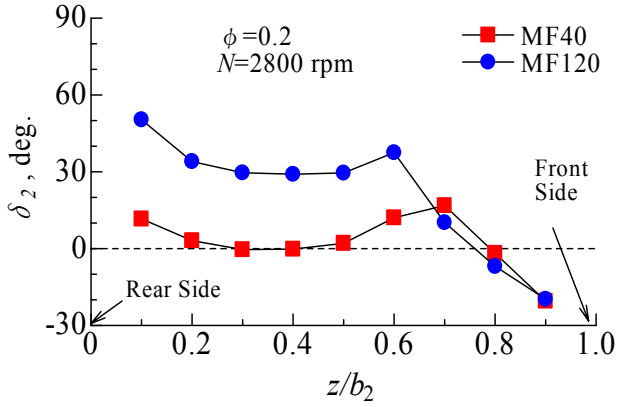

Fig. 15 Distribution of the deviation angle in the span direction

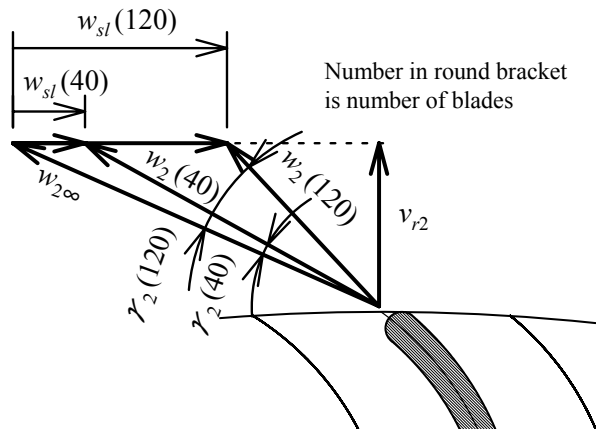

Fig. 16 Velocity triangle at the impeller outlet

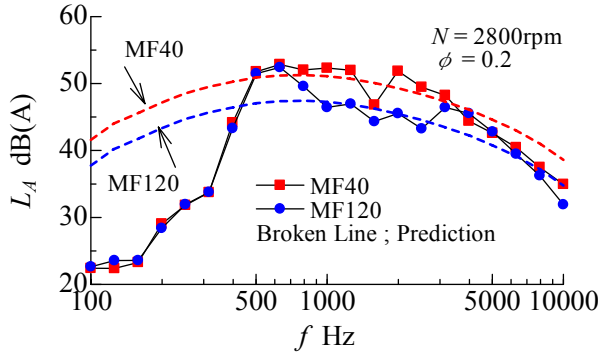

Fig. 17 Spectrum distribution of the fan noise

Table 4 Summary of the wake characteristics and noise levels

	MF40	MF120
Relative Velocity , w_2 m/s	13.4	12.0
Velocity Fluctuation , w_2'/w_2	0.140	
Ratio of Vortex Scale , ε	0.685	
Measured Noise Level , L_A dB	58.8	56.0
Predicted Noise Level , L_A dB	58.3	54.7

The relation between the flow coefficient and the fan noise is shown in Fig. 18. The measured fan noise of MF120 is 2.8 dB lower than that of MF40 in the vicinity of φ= 0.2. On the other hand, the total pressure coefficient of MF120 is lower than that of MF40 (see Fig. 13). In this case, the overall performance can be estimated by considering the specific noise.

Figure 19 indicates the relation between the flow coefficient and the specific noise level. The specific noise of MF120 is smaller than that of MF40 in the vicinity of design point. The measured and predicted characteristics are summarized in Table 5. According to this prediction, the fan noise of MF120 is 3.6 dB smaller than that of MF40; the specific noise of MF120 is 2.7 dB smaller than that of MF40. It has been quantitatively estimated that the deceleration in the relative velocity contributed to an improvement in the overall performance.

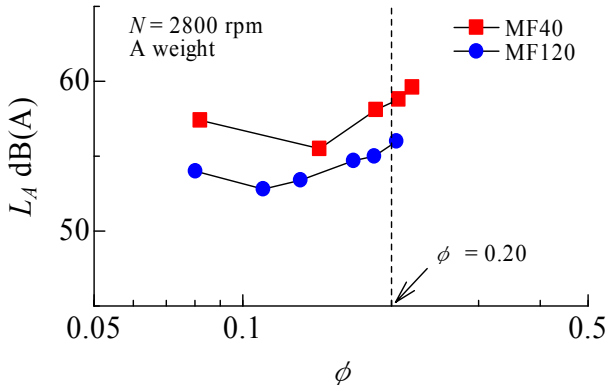

Fig. 18 Relation between the flow coefficient and fan noise

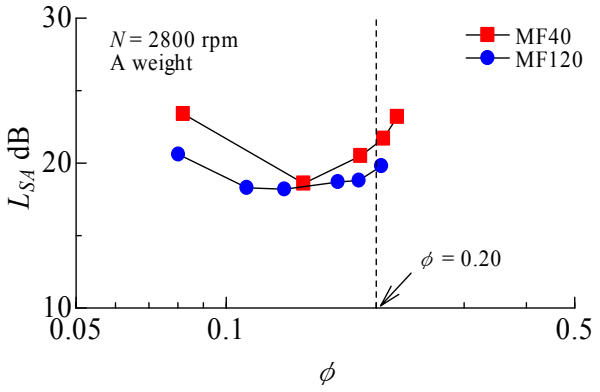

Fig. 19 Relation between the flow coefficient and specific noise

Table 5 Summary of the predicted characteristics of the forward curved fan

Fan	MF40		MF120	
	Measurement	Prediction	Measurement	Prediction
ϕ	0.20			
N , rpm	2800			
ϕ_t	1.76	1.75	1.55	1.58
L_A , dB (A)	58.8	58.3	56.0	54.7
L_{SA} , dB (A)	21.4	21.0	19.7	18.3

5. Conclusion

In this study, we proposed a prediction theory for specific noise by considering the internal flow of a forward curved fan. The specific noise levels of two fans having a different number of blades were predicted. The proposed theory was able to predict the values of total pressure, fan noise, and specific noise for the fan in the vicinity of the design point. On the basis of the results of the prediction, the following conclusions about the relationship between the overall performance and the internal flow were obtained.

(1) The flow around the impeller with 120 blades (MF120) was more biased than that around the impeller with 40 blades (MF40). On the other hand, the vortex flow domain of MF120 was narrower than that of MF40. An effective domain of the energy

conversion of MF40 has extended overall than MF120.
(2) It was observed that the decrease in the total pressure was affected by the slip factor and the pressure loss of the vortex flow. The increase in the total pressure at MF40 was attributed to the suppression of a major drop in the pressure and the expansion of the effective domain for energy conversion.
(3) The position around the impeller for which the relative velocity became maximum was different for each fan. That is, the position of the flow phenomena around the impeller that behaves as the source of fan noise is not necessarily the same for all fans. At the position of the noise source, the deviation angle in the main flow domain of MF120 was larger than that of MF40. The relative velocity of MF120 was also less than that of MF40 because of the slip.
(4) Based on the internal flow of the forward curved fan, it was predicted that the specific noise of MF120 was 2.7 dB less than that of MF40. It has been quantitatively estimated that the deceleration in the relative velocity contributed to the improvement in the overall performance.

Nomenclature

a_0	speed of sound (m/s)
B	number of blades
b	span length (mm)
C	chord (mm)
C_L	lift coefficient
c_{sl}	slip velocity (m/s)
D_{SS}	width of share layer (mm)
D^*	width of wake (mm)
D_1	inner diameter (mm)
D_2	outer diameter (mm)
F	lift (N)
f	frequency (Hz)
H	height of scroll casing (mm)
K_r	projection ratio
K_z	vortex flow coefficient
K_w	wake coefficient
K_θ	biased flow coefficient
k	slip factor
L	length of separation domain (mm)
Ls	scale of vortex in span length (mm)
L_A	noise level (dB(A))
L_{SA}	specific noise level (dB)
N	number of rotation (rpm)
P_t	total pressure (Pa)
p	sound pressure (Pa)
p_o	base sound pressure (Pa)
Q	flow rate (m^3/min)
Re	Reynolds number
r	distance from sound source to the observation point (m)
S_t	Strouhal number
u	tangential velocity
v_r	radial component of absolute velocity (m/s)
v_θ	circumferential component of absolute velocity (m/s)
W	width of scroll casing (mm)
w	relative velocity (m/s)
w'	velocity fluctuation of relative velocity (m/s)
z	coordinate of span direction (m)
β	relative flow angle (deg.)
β_b	outlet angle of impeller (deg.)
Γ	circulation (m^2/sec)
γ	deviation angle (deg.)
δ	thickness of boundary layer (m)
$\Delta\psi_w$	pressure loss coefficient of wake
$\Delta\psi_{vf}$	pressure loss coefficient of vortex flow
ε	ratio of vortex structure
θ	angle around scroll casing (deg.)
κ	intermittency factor
λ	aspect ratio of wake vortex
ρ	density (kg/m^3)
$\Sigma\triangle\psi$	total pressure drop
φ	flow coefficient
ψ_t	total pressure coefficient
$\psi_{th\infty}$	Euler's total pressure coefficient
$\psi_{th} = \psi_{th\infty} - 2k_2$	theoretical total pressure coefficient
ω	angular velocity (rad./s)

subscript

1	inlet side of impeller
2	outlet side of impeller
$\overline{\ }$	root mean square or ensemble average in main flow domain
PS	pressure surface side
SS	suction surface side

References

[1] Japanese Standards Association, 2002, "Glossary of terms for fans, blowers and compressors," JIS B 0132 (in Japanese), p. 459.
[2] Kind, R. J. and Tobin, M. G.., 1990, "Flow in a Centrifugal Fan of the Squirrel-Cage Type," ASME Journal of Turbomachinery, Vol. 112, No.11, pp. 84-90.
[3] Kind, R. J. 1997, "Prediction of Flow Behavior and Performance of Squirrel-Cage Centrifugal Fans Operating at Medium and High Flow Rates," ASME Journal of Fluids Engineering, Vol. 119, No. 3, pp. 639-646.
[4] Velarde-Suárez, S., Santolaria-Morros, C., and Ballesteros-Tajadura, R., 1999, "Experimental Study on the Aeroacoustic Behavior of a Forward-Curved Blades Centrifugal Fan," ASME Journal of Fluids Engineering, Vol. 121, No. 2, pp. 276-281.
[5] Velarde-Suárez, S., Ballesteros-Tajadura, R., Hurtado-Cruz, J. P., and Santolaria-Morros, C., 2006, "Experimental determination of the tonal noise sources in a centrifugal fan," Journal of Sound and Vibration, Vol. 295, pp. 781-796.
[6] Velarde-Suárez, S., Ballesteros-Tajadura, R., Santolaria-Morros, C., and Pereiras-García, B., 2008, "Reduction of the aerodynamic tonal noise of a forward-curved centrifugal fan by modification of the volute tongue geometry," Applied Acoustics,

Vol. 69, No. 3, pp. 225-232.
[7] Sasaki, S., Kodama, Y., Hayashi, H., and Uto, T., 2006, “Influence of Solidity on Total Pressure Characteristic of a Multiblade Fan, “ Turbomachinery (in Japanese), Vol.32, No.12, pp. 739-747.
[8] Schlichting, H., 1968, “Boundary-Layer Theory,” McGraw-Hill Book Company, 6th Edition, pp. 135-148
[9] Johnston, P., Dean, Jr., P., 1966, “Losses in Vaneless Diffusers of Centrifugal Compressors and Pumps,” ASME Journal of Engineering for Powers, Vol. 88, No.1, pp. 49-62.
[10] Curle, N., 1955, “The Influence of the Solid Boundary upon Aerodynamic Sound,” Proceedings of Royal Society of London, A231, pp. 505-514.
[11] Fukano, T. and Talukder, 1986, “A. A., Discrete Frequency Noise Generated form an Inclined Flat Plate Immersed in a Uniform Oncoming Flow,” Transactions of the Japan Society of Mechanical Engineers, Series B (in Japanese), Vol. 52, No. 480 , pp. 2828-2836.
[12] Iida, A., Fujita, H., Kato, C., and Takano, Y., 1995, “Experimental Investigation of Generation Mechanism of Aerodynamic Noise: 1st. Report, On a Coherent Structure of Surface Pressure Fluctuation on a Circler Cylinder,” Transactions of the Japan Society of Mechanical Engineers, Series B (in Japanese), Vol. 61, No. 592 ,pp. 4371-4378.
[13] Sasaki, S. and Kodama, Y., 2003, “The Standing Wake Formed in the Wake of a Flat Plate Blade and the Coherent Structure,” Journal of Japan Society of Fluid Mechanics (in Japanese), Vol. 22, No. 4, pp. 325-335.
[14] Japanese Standards Association, 2005, “Glossary of terms for fans, blowers and compressors,” JIS B 0132 (in Japanese), p. 459.
[15] Sasaki, S., Hayashi, H., and Kodama, Y., “Application of Wake Characteristics to Prediction of Broadband Noise of a Multiblade Fan,” Proceedings of the 9th Asian International Conference on Fluid Machinery, Jeju, Korea, No. AICFM9-133.